C. Pérez-Aranda
Centro de Investigación Científica de Yucatán, A.C., Unidad de Materiales, Calle 43 No.130 × 32 y 34, Col. Chuburná de Hidalgo, Mérida, Yucatán 97205, Mexico
e-mail: Kaisar_1992@hotmail.com

R. Pech-Pisté
Centro de Investigación Científica de Yucatán, A.C., Unidad de Materiales, Calle 43 No.130 × 32 y 34, Col. Chuburná de Hidalgo, Mérida, Yucatán 97205, Mexico
e-mail: rulo742@gmail.com

H. J. Carrillo-Escalante
Centro de Investigación Científica de Yucatán, A.C., Unidad de Materiales, Calle 43 No.130 × 32 y 34, Col. Chuburná de Hidalgo, Mérida, Yucatán 97205, Mexico
e-mail: hugojoel@cicy.mx

G. C. Uribe-Riestra
Centro de Investigación Científica de Yucatán, A.C., Unidad de Materiales, Calle 43 No.130 × 32 y 34, Col. Chuburná de Hidalgo, Mérida, Yucatán 97205, Mexico
e-mail: gabyuriber@gmail.com

F. Avilés[1]
Centro de Investigación Científica de Yucatán, A.C., Unidad de Materiales, Calle 43 No.130 × 32 y 34, Col. Chuburná de Hidalgo, Mérida, Yucatán 97205, Mexico
e-mail: faviles@cicy.mx

Thermo-Mechanical Properties of Carbon Nanotube Yarns With High Energy Dissipation Capabilities

Carbon nanotube yarns (CNTYs) are porous hierarchical fibers that exhibit a strong property-structure relationship. The morphology and structure of dry-spun CNTYs are characterized and correlated with their quasi-static and dynamic mechanical properties. These characterizations include assessment of the CNTY homogeneity by means of Raman spectroscopy mapping, determination of linear density and porosity, atomic force microscopy, and dedicated measurements of the statistical distribution of the yarn's diameter. Tensile testing of CNTYs yielded a specific strength of 0.21–0.34 N/tex, and a specific elastic modulus of 3.59–8.06 N/tex, depending on the gage length. While the strength is weakly sensitive to the gage length, the elastic modulus depends on the gage length. The importance of subtracting the machine compliance for the determination of the CNTY's elastic modulus is highlighted, since the error can reach up to 28%. Dynamic mechanical analysis shows that the CNTY is a stiff material with an extraordinary high damping ratio, which increases with temperature and reaches ~0.6 at 60 °C. In addition, the CNTY presents a frequency-stiffening behavior in the 18–48 Hz range, with storage modulus (E′) and loss modulus (E″) which increase ~2.5 times (E′) and ~7 times (E″) at 48 Hz. [DOI: 10.1115/1.4055540]

Keywords: carbon nanotube yarns, mechanics, mechanical properties, dynamic mechanical analysis, damping, elastic behavior, mechanical behavior, microstructure-property relationships

1 Introduction

Carbon nanotube (CNT) yarns (CNTYs) are continuously long, porous, and twisted fibers, made of thousands of highly aligned CNTs in their cross section, whose bundles are held together by van der Waals forces and CNT entanglement [1–4]. CNTYs have a hierarchical structure since the strong intermolecular forces between CNTs (building blocks) yield interlocked structures called bundles, which are dry-spun with a twist angle to form the continuous fiber [4,5]. Hypothetically, CNTYs could reach properties similar to those of the CNTs that make them up, which makes this novel material very attractive for engineering applications. Dry-spun CNTYs exhibit outstanding properties such as low density, large surface area, high electrical conductivity (10^4–10^5 S/m) [2,6–11], elastic modulus ranging from 1.6 GPa to 330 GPa, and tensile strength around 0.05–3 GPa [2,7,12–17]. This combination of properties encourages their inclusion in other engineering textiles and polymeric matrices to develop multifunctional structural devices that can generate and store energy, sense, and respond to external stimuli, such as capacitors, batteries, artificial muscles, sensors, and actuators [9,18].

Because of their hierarchical structure (CNTs, bundles, fibrils, yarn) and current synthesis methods, CNTY properties are very sensitive to their architecture at the nano- and micro-scales, including the length of the individual nanotubes, bundle thickness, porosity, and twist angle [9]. Such a strong property-structure relationship may yield not only batch-to-batch property variations, but some structural properties may also vary within the same yarn [14,19]. Thus, statistical methods and/or property mapping may be needed to better characterize the CNTYs. Ultimately, the yarn's architecture is responsible for the effective properties (mechanical and dynamic mechanical) of the yarn, and such properties are affected by

[1]Corresponding author.

Contributed by the Materials Division of ASME for publication in the Journal of Engineering Materials and Technology. Manuscript received March 8, 2022; final manuscript received September 1, 2022; published online September 23, 2022. Assoc. Editor: Tariq Khraishi.

temperature. Materials in engineering commonly present either high stiffness (e.g., metals) or high energy dissipation capabilities (e.g., polymer foams), but a combination of both is rarely found. The development of materials with high stiffness and high energy dissipation capabilities is yet a current challenge for research in materials engineering, and a great area of opportunity for applications related to vibrations, structural damping, fatigue, and durability [20,21]. In this respect, CNTs have shown remarkable mechanical and multifunctional properties, and also have the capability of being assembled into macroscopic structures (arrays, buckypapers, aerogels, and fibers) that aim to retain the outstanding properties of individual CNTs [3,21].

The interconnected morphology of CNT assemblies may render several structural viscoelastic mechanisms upon loading/unloading (zipping/unzipping, self-organization, bundle sliding), which are prone to enhance their damping performance [9,20,21]. Among the CNT arrays, CNTYs are of particular attention for structural applications in the composites industry, because of their continuous fibrillary form and high specific mechanical properties [4,22]. The tensile response of individual CNTYs has been investigated to some extent [7,11–16,23], although the effect of the fiber (coupon) gage length and machine compliance have been downplayed. A few studies report the influence of the gage length on the tested mechanical properties [14,15], but none of them accounts for the effect of the testing machine compliance. This is important given that commonly employed tensile test methods for such fibers depend on the crosshead displacement of the testing machine used for measuring force/strain [24,25]. Dynamic mechanical analysis (DMA) of CNTYs is experimentally challenging given the micrometric diameter of the fibers and their porous architecture, so very few DMA studies of CNTYs have been published [21,26,27]. Understanding the (quasi-static) mechanical and dynamical responses of CNTYs and their relationship with their microstructure will allow a better understanding of the structure-property relationship of such novel carbon materials.

Given this motivation, this work focuses on investigating the mechanical and damping properties of dry-spun CNTYs using tensile testing and DMA. Individual yarns are DMA-tested under cyclic loading using temperature and frequency scans. For a better understanding of the mechanisms governing the dynamic response of the CNTYs, mechanical, thermogravimetric analysis (TGA), atomic force microscopy (AFM), and Raman spectroscopy mapping characterizations are conducted. Raman spectroscopy is also conducted in situ during tensile testing to shed light on the loading mechanisms. Due to the strong property-structure dependence of this hierarchical material, dedicated experiments were also conducted to meticulously characterize the morphological and structural properties (diameter, linear density, homogeneity) of the CNTYs.

2 Materials and Methods

2.1 Materials. The CNTYs used were synthesized at the Nanoworld Laboratories (Cincinnati, OH). They were dry-spun from the sides of 500 μm-high vertically aligned arrays composed of CNTs grown by water-assisted chemical vapor deposition. The CNTs have an outer diameter ranging from 9 nm to 12 nm and distribution of 2–3 walls [7,13]. Our measurements indicate that CNTYs have a twist angle of ~32 deg, which agrees with the data provided by the supplier. Three batches of yarns (10 m long each batch) were used, all of them synthesized under the same conditions and indicated as 25 μm diameter by the supplier. However, dedicated statistical measurements of the CNTY diameter for each batch indicated that a statistical distribution of diameters exists (20–70 μm), with slight batch-to-batch variations. Therefore, the mean (expected) value of the distribution was used for all tests or properties which required diameter as input, as will be further discussed.

2.2 Scanning Electron Microscopy and Diameter Distribution of Carbon Nanotube Yarns. Scanning electron microscopy (SEM) was carried out using a JEOL JSOL-6360-LV microscope (Tokyo, Japan). SEM images were obtained from the longitudinal section of the CNTYs with magnifications of 500× and acceleration voltages of 20–25 kV. In order to construct a statistical diameter distribution of the CNTYs, 20 values of diameter were acquired for each of the 14 SEM images, obtaining a total of 280 diameter measurements per batch (three batches total). Diameters were calculated from SEM images using the ImageJ software (National Institute of Health, Montgomery, AL), and the statistical analysis of the data was performed using the minitab software (Minitab, LLC, State College, PA). The analysis comprised the assessment of several statistical probability distributions, viz. normal, log-normal, Gamma, and two- or three-parameter Weibull, whose probability density functions and moments are presented in Sec.S1 available in the Supplemental Materials on the ASME Digital Collection. The distribution function was chosen according to the Anderson–Darling goodness-of-fit test, which determines whether the experimental diameter distribution followed the evaluated distribution [28]. The selected distribution was the one with the lowest Anderson–Darling value. Finally, the expected (or mean) value (μ_e), median (μ_n), and mode (μ_o) were calculated with the selected distribution. Mean values (μ_e) were used for any subsequent calculation which requires diameter as input (e.g., DMA).

2.3 Atomic Force and Scanning Electron Microscopy. The CNTYs were morphologically characterized by AFM, using an SPM-8 equipment from Bruker (Kontich, Belgium). Different sections of $3\times3\ \mu m^2$ and $10\times10\ \mu m^2$ of the CNTYs were scanned, using tapping mode (dynamic contact mode) in the air. Surface roughness was measured using the NanoScope Analysis 1.5 from Bruker, using sub-areas of $5\times5\ \mu m^2$ of the $10\times10\ \mu m^2$ AFM images. The roughness is reported as the root mean square average of 24 measurements, acquired from six images of different sections of a CNTY (four measurements per image).

2.4 Raman Spectroscopy. Raman spectroscopy of individual CNTYs was carried out with a confocal Renishaw inVia Raman spectrometer (Wotton-under-Edge, England), using a 50× objective lens, a 633 nm (red) laser, 60 s exposure time, and 1800 lines/mm grating (spot size ~1 μm). A 100 μm line scan (from 0 μm to 100 μm with steps of 1 μm, for a total of 101 Raman spectra plots) was performed along the CNTY axial direction, to better assess the homogeneity of the structural composition of the CNTY. Each line analysis took about 7 h using the automated scanning function of the Renishaw Raman equipment. The Raman peaks were fitted to a Lorentz function to obtain the center position, the full width at high maximum (FWHM), and the intensity of the Raman bands. The mean and standard deviation values of the Raman parameters were obtained from the line scan Raman spectra using a total of 21 Raman plots (one every 5 μm).

In separate experiments, in situ Raman spectroscopy was conducted while straining the CNTY with a special test rig, in order to investigate the extent of C–C bond stretching in the CNTY during the early stages of loading. Details of the in situ test rig and results are included in Sec. S2 available in the Supplemental Materials on the ASME Digital Collection.

2.5 Linear Density and Porosity. To measure the CNTY weight accurately, three segments of the CNTYs with different lengths ($L = 60$, 120, and 180 mm) were weighed by the microbalance (0.1 μg resolution) of a Perkin Elmer TGA 7 thermogravimetric analyzer (Waltham, MA). The smallest CNTY length used was 60 mm, in order to allow sufficient mass in the microbalance. To guarantee uniformity in length between samples and prevent buckling of the fibers, the CNTYs were slightly preloaded using an in-house fixture by attaching a 75 mg mass at the end of the fiber. The linear density of the CNTYs (ρ_L), expressed as the mass of the fiber per unit length, was determined as the slope of

the best linear fit of the mass versus length plot, setting the intercept at (0,0). In addition, the porosity of the CNTYs (ϕ) was estimated according to [6,29]

$$\phi = 1 - \frac{\rho_{CNTY}}{\rho_{CNT}} \tag{1}$$

where ρ_{CNT} is the bulk density of a CNT and ρ_{CNTY} is the measured density of the CNTY. The CNT density was calculated as [30]

$$\rho_{CNT} = \frac{4}{1{,}315{,}000}\left[\frac{n}{d_{Out}} - \frac{2d_{S-S}\sum_{i=0}^{n-1} i}{d_{Out}^2}\right] \tag{2}$$

where n is the number of CNT walls ($n = 3$ was used in our case, since it is the most frequently observed value), d_{S-S} is the intershell distance of the CNTs (0.34 nm), and d_{Out} is the CNT outer diameter (11 nm).

The volumetric density of the CNTY was obtained by dividing its linear density by its cross-sectional area (using the mean diameter of the statistical distribution).

2.6 Thermogravimetric Analysis. TGA in nitrogen atmosphere was performed in a Perkin Elmer TGA 7 thermogravimetric analyzer (Waltham, MA) for samples with a length of ~1 m. First, a preheating scan was carried out with a heating rate of 10 °C/min from 30 °C to 400 °C, to eliminate adsorbed moisture and potentially residual byproducts generated during CNTY synthesis. Then, a full temperature scan was applied up to 800 °C, using identical conditions.

2.7 Uniaxial Tensile Testing. Single-filament CNTYs were tested in uniaxial tension under monotonically increasing load using a tabletop Shimadzu AGS-X (Kyoto, Japan) universal testing machine, with a crosshead displacement of 0.5 mm/min. The tensile specimens consist of a single CNTY bonded onto a cardstock frame with a rectangular internal window, Fig. 1. The ends of the fibers were fixed to the frame using a cyanoacrylate adhesive and the frame was cut at the middle before running the test, as advised in Refs. [24,25]. The strain calculated from the crosshead displacement of the testing machine includes contributions from the load cell and gripping system, fact that is frequently overlooked. Therefore, to accurately determine the strain of the CNTYs, the system compliance (C_s) was calculated and subtracted from the apparent compliance of the specimen (C_a) to obtain true specimen compliance [24,25]. For this purpose, mechanical tests were carried out following the guidelines of the ASTM D3379 [24], which suggest conducting tensile testing over a range of gage lengths. Thus, three gage lengths ($L_g = 12.5$, 25, and 37.5 mm) were tested by scaling the dimensions recommended in the ASTM standard, as shown in Fig. 1. Ten specimens (replicates) per each fiber length were tested, and representative load–displacement curves are shown in Sec. 3. For each specimen, the value of C_a was obtained as the inverse of the initial slope of the load (P) versus the displacement (ΔL_g) curve in the $0.06\ \text{mm} \le \Delta L_g \le 0.40\ \text{mm}$ range. Then, the slope of the C_a versus L_g plot was identified as m, and C_s was determined as the intercept of C_a at $L_g = 0$. Finally, the fiber axial elastic modulus, independent of L_g, was calculated from the slope (m) and cross-sectional area of the CNTY (A) as [25]

$$E = \frac{1}{mA} \tag{3}$$

2.8 Dynamic Mechanical Analysis. DMA tests of individual CNTYs were carried out using a Perkin Elmer DMA 7 dynamic mechanical analyzer (Waltham, MA). Test specimens consisted of a single CNTY bonded onto a commercial polyimide frame with a rectangular internal window, as shown in Fig. 2(*a*). The total length of the fiber was 14 mm, and the gage length was 8 mm. For temperature (T) scans, the CNTYs were tested under cyclic loads at uniaxial tension (1 Hz frequency), from −50 °C to 300 °C, with a heating rate of 5 °C/min. Frequency (f) scans were performed from 0.1 Hz to 48 Hz at different constant temperatures (−50 °C, 30 °C, 50 °C, and 100 °C). The values of the static (F_S) and dynamic (F_D) forces needed for the test, see Fig. 2(*b*), were first calibrated in initial tests not discussed herein. The dynamic force was taken as 70% of the static force, i.e., $F_D = 0.7\ F_S$, oscillating sinusoidally around F_S, as depicted in Fig. 2(*b*) ($F_{Max} = F_S + F_D$, $F_{Min} = F_S - F_D$). The possible effect of F_S was first investigated by initially considering three values of such a static force, viz. 18 mN, 30 mN, and 50 mN. Considering that the average failure load of the CNTY (F_{Fail}, determined from quasi-static testing, Sec. 2.7) is $F_{Fail} = 109$ mN, these values of F_S correspond to $F_{Max}/F_{Fail} = 28.1\%$, 46.8%, and 78.0% (respectively). The initial tests showed premature failure of the CNTYs for $F_S = 50$ mN, and differences in the response curves that are within the experimental scattering for $F_S = 18$ mN and 30 mN. Therefore, the final conditions used (those reported herein) were set to $F_S = 18$ mN and $F_D = 12.6$ mN. The resulting strains ranged from 1% to 3%. Measurements of a large number of specimens tested with different static forces are shown in Fig. S4 available in the Supplemental Materials on the ASME Digital Collection.

3 Results and Discussion

3.1 Morphological and Structural Properties of the Carbon Nanotube Yarns

3.1.1 Diameter Distribution. A representative SEM image of the CNTY used for diameter measurements is shown in Fig. 3.

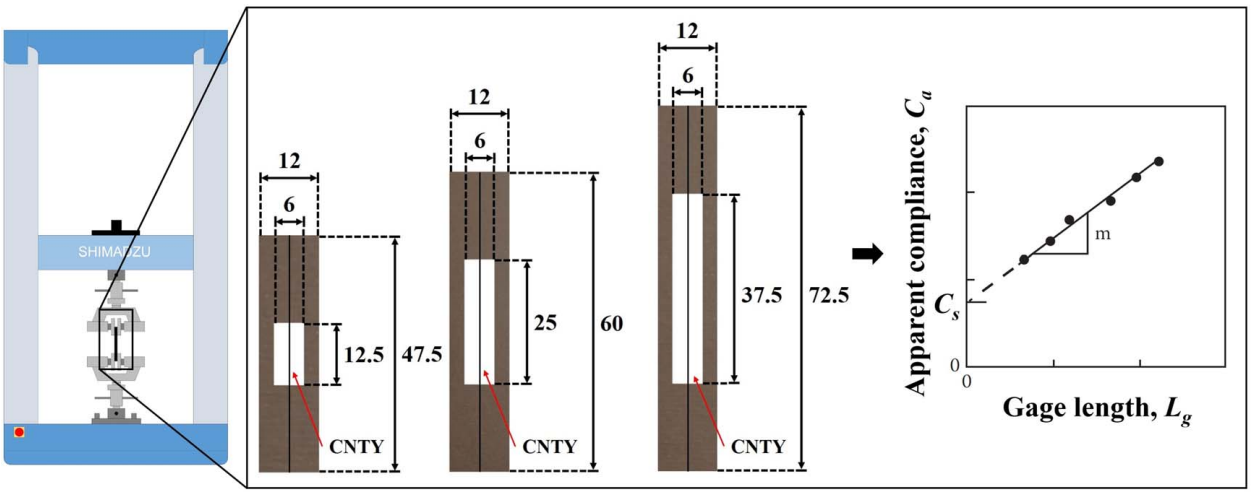

Fig. 1 Schematic of the experimental setup used for tensile testing of CNTYs, showing the data reduction. Dimensions in mm.

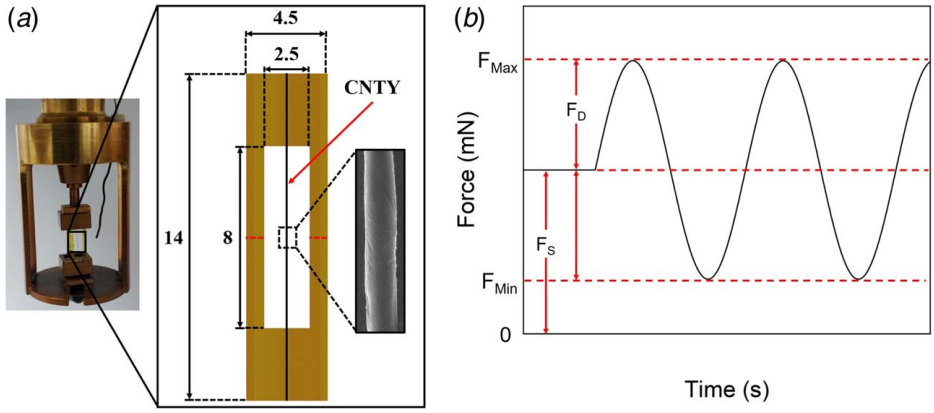

Fig. 2 Dynamic mechanical analysis of the CNTYs: (*a*) experimental setup (dimensions in mm) and (*b*) schematic of the oscillatory force

For each SEM image, 20 measurements (~12 μm apart) were taken through the length of the CNTY. However, for visualization purposes, only four diameter measurements are marked in Fig. 3(*a*). From this figure, it is observed that the morphology of the CNTY consists of CNT bundles/fibrils with an angle of inclination (twist angle) with respect to the longitudinal direction of the CNTY. Twenty measurements of the twist angle indicated average and standard deviation of 32.2 deg $\pm$6.9 deg. It is observed that the CNTY has significant variations of diameter through its length, which is attributed to a non-perfectly uniform rotation rate of the spinning machinery during the drawing process [29]. This yields a CNTY diameter that may vary even within the same batch. As indicated in Fig. 3(*b*), for the same batch the fiber diameter may vary from 32 μm to 56 μm, with most of the data (~80%) between 36 μm and 46 μm. Similar variations, but with slightly different statistical distributions were found for the other two batches (10 m long batches) examined, as shown in Sec. S1 available in the Supplemental Materials on the ASME Digital Collection.

Since the value used as diameter affects the calculation of several properties of the CNTY reported herein (elastic modulus, storage and lost modulus, volumetric density, etc.), rigorous statistical quantification was performed by fitting several statistical distributions to the experimental data, as shown in the example of Fig. 3(*b*).

The Anderson–Darling goodness-of-fit test with a 99% confidence level showed that the diameter distribution could be fitted to a three-parameter Weibull distribution (fitting line in Fig. 3(*b*)). The Anderson–Darling value (0.96) for the three-parameter Weibull distribution was the smallest among those obtained for the other distributions, such as Gamma and log-normal, see Table S2 available in the Supplemental Materials on the ASME Digital Collection. By using the parameters of shape, scale and location, and the moment equations listed in Table S1 available in the Supplemental Materials on the ASME Digital Collection, the three-parameter Weibull distribution for the fiber shown in Fig. 3(*a*) yields $\mu_e = 42.3$ μm, $\mu_n = 41.9$ μm, and $\mu_o = 41.0$ μm. The expected (or mean) value (μ_e) was used for all subsequent characterization needing the diameter. Overall, three batches of CNTYs were employed for mechanical testing and DMA, and the same statistical analysis was performed to determine the mean diameter of each batch.

3.1.2 Surface Roughness and Estimation of Bundle Thickness. Figure 4 shows an AFM topography of the CNTY. It is noticed that the surface of the CNTYs is very porous, comprising CNT fibrils/bundles which are generally parallel-oriented and entangled. The diameter (thickness) distribution of the CNT bundles comprising the CNTY is broad, and the measurement of several AFM images resulted in a range of 99–436 nm. It is common to observe a wide range of CNT bundle diameters in CNTYs, see e.g., Refs. [31,32]. The root mean square roughness of the CNTYs, in this case, is 62.2 ($\pm$12.5) nm. This is a very high value, compared with typical values reported for conventional carbon fibers (2.6–12.5 nm [33,34]).

3.1.3 Raman Spectra. Figure 5(*a*) shows the Raman line spectra of a 100 μm region along the longitudinal direction of the CNTY, at its central region. For the line analysis, data were taken every 1 μm, so there are 101 Raman spectra plotted in Fig. 5(*a*). Each of the 101 spectra shows the same characteristic peaks as those in Fig. 5(*b*), which is a representative Raman spectrum of a random location along the fiber. The presence of a small radial breathing mode (RBM) band at ~100–500 cm^{-1} (see Fig. 5(*b*)), indicates the presence of a few single-wall (SWCNTs) or double-wall CNTs (DWCNTs) comprising the CNTY [19,35–39]. The

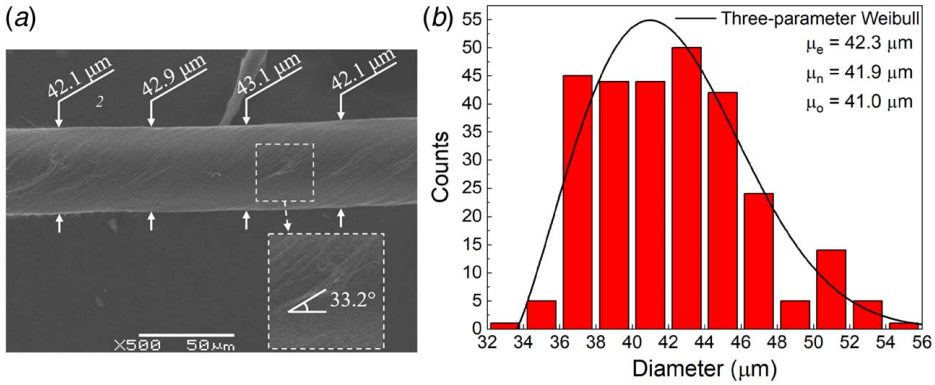

Fig. 3 Diameter distribution of the CNTY: (*a*) SEM image and (*b*) histogram and fitting curve

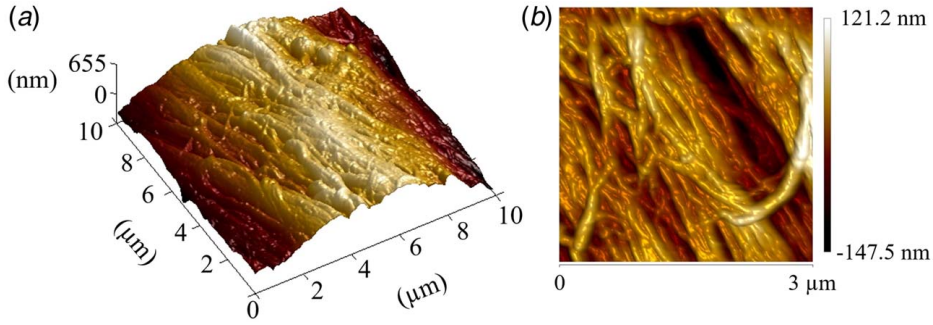

Fig. 4 AFM images of different sections of a CNTY: (*a*) three-dimensional image ($10 \times 10\ \mu m^2$) and (*b*) two-dimensional image ($3 \times 3\ \mu m^2$)

small intensity of this band confirms that the CNTY comprise mostly CNTs of three walls. Using the Raman shift localization of the RBM band ($\omega_{RBM} = 187.4\ cm^{-1}$, see Table 1), and the relation $d_{CNT} = (248\ cm^{-1}\ nm)/\omega_{RBM}$ [19,36,40], it is found that the SWCNTs have an approximate diameter (d_{CNT}) of ~1.3 nm.

The weak band at ~600 cm^{-1} is produced by combination modes related to the double resonance process, known as intermediate frequency phonon modes [40,41]. The band at ~1330 cm^{-1} corresponds to the so-called D band (disordered-induced), which arises from the in-plane breathing vibrations of the aromatic ring structures. The D band is induced by the presence of disorder of the crystalline structure of the CNTs or vacancies in the graphitic structure through double resonance Raman processes [35,41–44]. The band at ~1585 cm^{-1} corresponds to the G band (graphitic), which arises from the in-plane bond stretching motion of pairs of sp^2 hybridized carbon atoms [41,43,44]. The G band is asymmetric towards lower Raman shift values, which confirms the presence of CNTs with few walls [19]. It has also been pointed out that the Raman shift position of the G band can be used to determine residual strains induced in the CNTs during the CNTY assembly process [19]. In addition, the relative intensity of the D to G bands (I_D/I_G) provides information on the degree of disorder in sp^2 carbon materials [35,41] and can be used to further assess the homogeneity of the composition of the CNTY. According to the data in Table 1, the CNTYs present a ratio $I_D/I_G = 1.70 \pm 0.08$, which is within the interval of those reported for other CNTYs [12,45]. This value can be ascribed to a high number of symmetry-breaking features in the CNTs comprising the yarn, most likely induced during the CNTY manufacturing process. The peak at ~2650 cm^{-1} is the so-called 2D (or G') band. The G' band is an overtone of the D band, i.e., a second-order two-phonon process [41,43,44,46]. A relatively high intensity value of the G' band is indicative of a metallic feature of the CNTs [47]. In DWCNT, the G' band can split into two components, G'_1 and G'_2 (Fig. 5(*a*)), corresponding to double resonance processes occurring at the inner and outer walls of the DWCNT, respectively [37,48]. Finally, the G + D band at ~2930 cm^{-1} is caused by two-phonon defect-assisted processes due to the presence of symmetry-breaking defects in the CNTY [41,44].

Regarding the Raman line spectra, moderate variations in intensities, position, and peak shapes were observed among the 101 Raman spectra. These variations correlate with the homogeneity of the yarn. Table 1 shows the average and one standard deviation values of the position, FWHM, and intensity of the characteristic Raman bands shown in Fig. 5(*b*), obtained by fitting the bands to Lorentzian functions. The standard deviation of the band position was less than 8.6 cm^{-1} for all bands, which is indicative of homogeneity in the chemical composition of the CNTY. This homogeneity can also be observed in the intensity ratio, which presents a standard deviation of ±0.08. The FWHM, on the other hand, presents larger scattering along the scanned line (100 μm), indicating variations in the structural composition of the yarn. Given the different CNTs that typically comprise a yarn (SWCNTs, DWCNTs, and multiwall CNTs (MWCNTs)), the Raman fingerprint of a CNTY could vary from position to position [19]. During CNTY manufacturing, CNTs may also be pre-stressed [19] and the degree of this pre-stress may vary from position to position within the yarn.

3.1.4 Linear Density and Porosity. The mean and one standard deviation values of the mass measured for the different CNTY

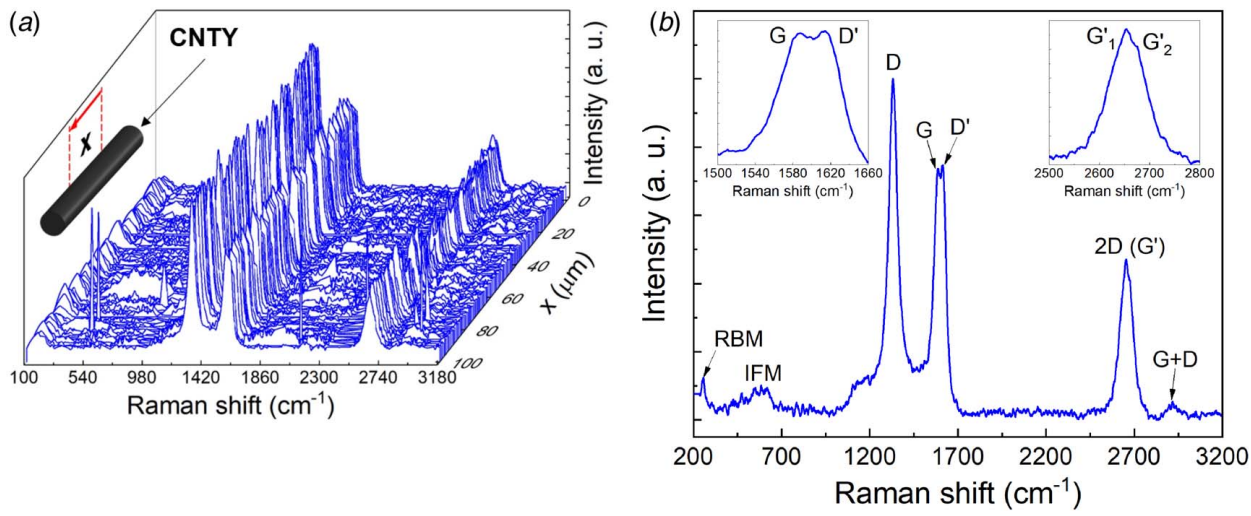

Fig. 5 Raman spectra of the CNTYs: (*a*) 100 μm line scan and (*b*) representative Raman spectrum

Table 1 Statistics of the Raman bands obtained from the CNTY line spectra

Raman band	Center position (cm^{-1})	FWHM (cm^{-1})	Intensity ratio
RBM	187.4 ± 2.79	85.8 ± 7.36	—
D	1331.6 ± 0.44	50.5 ± 5.04	$I_D/I_G = 1.70 \pm 0.08$
G	1584.3 ± 0.70	43.4 ± 5.27	—
D'	1619.8 ± 0.83	30.1 ± 1.50	—
2D (G')-G'$_1$	2629.8 ± 5.18	51.8 ± 5.08	—
2D (G')-G'$_2$	2671.8 ± 2.82	38.2 ± 12.6	—
G + D	2927.5 ± 8.60	68.8 ± 20.8	—

lengths ($L = 6$, 12, and 18 cm) and the corresponding linear fit (solid line) are shown in Fig. 6.

The values of CNTY mass increment with its length in a linear fashion. Thus, a linear density (ρ_L) can be calculated from the slope of the linear fit of the data [6], which in this case yields $\rho_L = 0.42$ tex (1 tex = 1 μg/mm). The linear density of CNTYs strongly depends on their diameter and porosity, and values of ρ_L between 0.10–0.82 tex (twisted) and 0.01–0.40 tex (untwisted) have been reported for dry-spun CNTYs [2,3,6,7,17,49]. Values of ρ_L between 0.03 tex and 1.40 tex have also been reported for direct spinning CNTYs [17,50,51]. By using the mean diameter determined from the statistical analysis (37.9 μm for batch C, see Sec. S1 available in the Supplemental Materials on the ASME Digital Collection), and assuming a solid cross section, the volumetric density of the CNTY yields $\rho_{CNTY} = 0.37$ g/cm^3. According to the supplier [52], the majority of the CNTs that comprise the CNTY have a diameter of ~11 nm and three or two walls. Raman spectroscopy conducted herein, and transmission electron micrographs provided by the supplier (not shown) indicate the dominance of CNTs with three walls. Thus, according to Eq. (2), and considering $n = 3$, the volumetric density of the CNTs is $\rho_{CNT} = 0.78$ g/cm^3. Applying Eq. (1), the calculated porosity of the CNTY is $\phi = 0.53$, which indicates that 47% of the yarn is composed of CNTs and the rest corresponds to empty spaces. On the other hand, if CNTs of two layers are considered ($n = 2$), $\rho_{CNT} = 0.54$ g/cm^3 and $\phi = 0.68$. Porosities of several other types of CNT fibers and yarns have been reported in the range of 0.40–0.90 [6,7,49].

3.2 Thermogravimetric Analysis. A representative TGA thermogram of the CNTYs including a preheating curve (solid squares), a full scan (empty circles), and the absolute value of its derivative (solid triangles) are shown in Fig. 7. In this analysis, the CNTY was first preheated from 30 °C to 400 °C, brought back to 30 °C (the mass remaining in the crucible was calibrated back to zero at this point), and immediately heated to a full scan

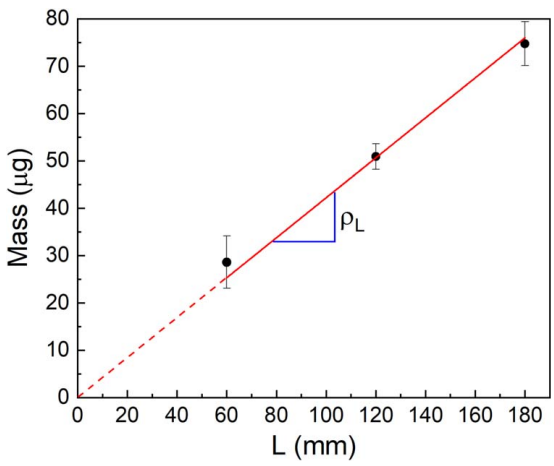

Fig. 6 Linear density (ρ_L) of the CNTYs

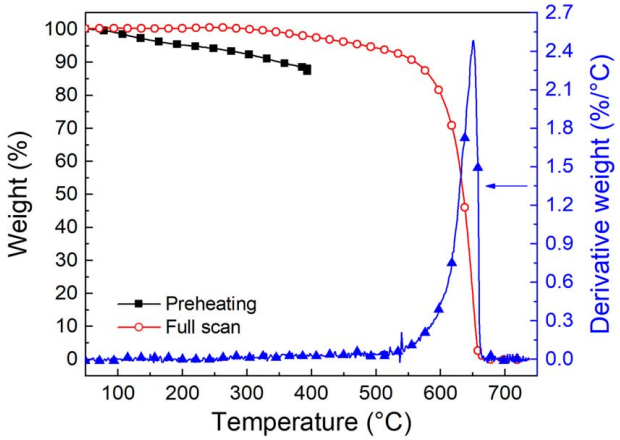

Fig. 7 TGA response of the CNTY

from 30 °C to 800 °C, without opening the TGA equipment. As shown in Fig. 7, during preheating the CNTY loses up to ~13% in weight at 400 °C. The initial weight loss ($T < 100$ °C) is attributed to the evaporation of both, the densifier (acetone) used in the fiber synthesis process and adsorbed moisture [53]. Subsequent weight losses at higher temperatures (150 °C < T < 400 °C) are ascribed to thermal degradation of amorphous carbon and other carbonaceous forms, because of its lower activation energy for the degradation process compared with more ordered structures [53–55]. Once those byproducts are thermally degraded, the subsequent full scan shows that the CNTY loses negligible weight (less than 1%) below ~350 °C, and only around 5% between 350 °C and 550 °C; this could be related to the elimination of remnants of amorphous carbon. Differences between the preheating and full scan at the same temperature range suggest that synthesis byproducts and amorphous carbonaceous materials in the CNTY have been eliminated during preheating, remaining only (or majorly) the CNTs comprising the yarn. From ~550 °C to 670 °C, the CNTY experiments a rapid mass loss, and the peak in derivative identifies the maximum decomposition temperature at ~650 °C. This is mainly attributed to the thermal decomposition of the CNTs and matches what has been observed in the literature for other CNTs and CNTYs [51,56]. The high thermal stability of the CNTYs can be linked back to the aromatic bonding of the CNT structure. The number of CNT walls and defects, the presence and composition of the catalyst, and the presence of other carbonaceous materials such as amorphous carbon and graphite particles, play a paramount role in the thermal stability of CNTYs [39,57].

3.3 Tensile Response at Different Gage Lengths. The mechanical response of CNTYs subjected to uniaxial tensile loading is shown in Fig. 8. This figure plots representative curves of load (P) versus crosshead displacement (ΔL_g) for each of the three gage lengths (L_g) investigated (ten specimens were tested for each gage length). The P–ΔL_g curves for all gage lengths exhibit a nearly linear behavior, after a small initial load adjustment.

The dependence of the maximum load with gage length is small, but the maximum displacement and stiffness depend on the gage length. This is an important issue when testing fibers which arises because the displacement/strain is measured with the crosshead of the testing machine, as has been previously recognized [24,25]. However, the majority of the literature reporting mechanical testing of CNTYs has ignored the effect of the gage length and machine compliance [7,12,13,16,50], with only a few authors considering the influence of the gage length [14,15]. Notice that the strain rate may also affect the mechanical response of CNTYs [14].

Table 2 lists the mechanical properties obtained from the P–ΔL_g curves. The data reduction used encompasses both, the engineering (homogenized) and the textile approaches.

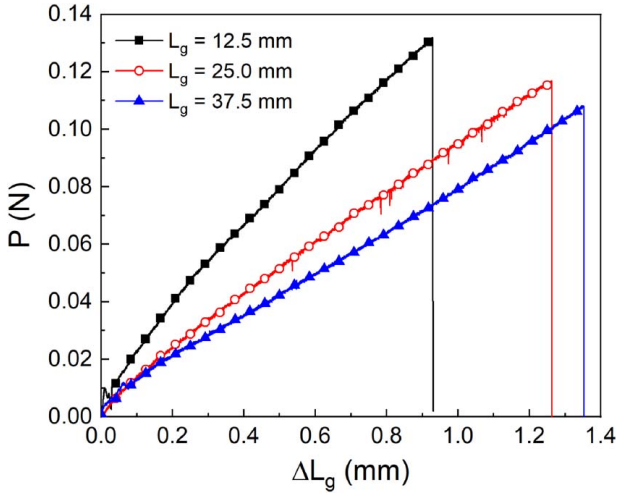

Fig. 8 Mechanical response of CNTYs under uniaxial tensile loading

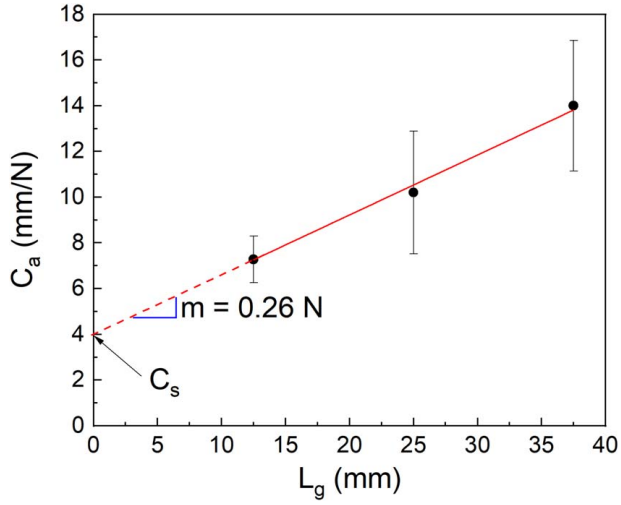

Fig. 9 Apparent compliance for three CNTY gage lengths

Table 2 Tensile mechanical properties of CNTYs

L_g	Specific strength (N/tex)	Apparent specific modulus (N/tex)	Tensile strength (MPa)	Apparent elastic modulus (GPa)	Apparent ultimate strain (%)
12.5	0.31 ± 0.03	4.15 ± 0.56	116 ± 10.2	1.55 ± 0.21	7.04 ± 0.88
25.0	0.26 ± 0.03	6.19 ± 1.60	95.3 ± 9.31	2.30 ± 0.60	4.36 ± 1.15
37.5	0.24 ± 0.03	6.57 ± 1.49	87.7 ± 10.8	2.44 ± 0.55	3.74 ± 0.83

The "engineering approach" assumes a continuous cross-sectional area for the calculation of the tensile strength and elastic modulus. This was conducted here using the mean diameter of the distribution reported in Sec. 3.1.1. However, as seen from the SEM (Fig. 3(*a*)) and AFM (Fig. 4(*a*)) images, CNTYs may present a non-uniform cross-sectional area, and are highly porous ($\phi = 0.53$–0.68, see Sec. 3.1.4), rather than continuous solids.

In addition, the calculated mechanical properties of the yarn using the engineering approach strongly depend on the diameter used for such calculations [29,49]. For those reasons, the mechanical properties of yarns are also listed by using the textile industry approach, based on the linear density, where diameter or volumetric properties are bypassed. The specific strength (also named "tenacity") is calculated by dividing the maximum load between the linear density, while the specific modulus is obtained from the slope of the best linear fit to the curve-specific strength versus strain. The mechanical properties in Table 2 using the engineering approach show that the (apparent) elastic modulus increases for longer gage lengths, while the tensile strength and (apparent) ultimate strain decrease. The reduction of the tensile strength for larger gage lengths has been previously observed and is attributed to the strength-limiting defects within the fiber [15]. The statistical presence of these defects promotes earlier failure as the gage length increases. Similarly, the specific properties (textile approach) show a small decrease in the specific strength and an increment in the specific elastic modulus for longer gage lengths. Since the strain and elastic modulus are obtained from the crosshead displacement of the universal testing machine, the values of elastic modulus calculated by this method carry certain errors, and hence they have been named as "apparent". This is because the measured compliance includes both, the compliance of the specimen and that of the testing machine (load cell and test rig) [25]. To correct for machine compliance, the measured (apparent) compliance (C_a) is plotted in Fig. 9 for the three gage lengths.

It is observed that C_a increases with increased L_g. The compliance of the whole test rig (system compliance, C_s) is determined from the intercept at $L_g = 0$ as 3.97 mm/N. From the slope of the linear fit ($m = 0.26$ N), Eq. (3) yields an elastic modulus of $E = 3.38$ GPa. This elastic modulus is independent of the gage length and is corrected for the effect of machine/test rig compliance.

Notice from Table 2 that, if this correction for machine compliance is not conducted, the uncertainty in E could be as large as 28%.

Given that a strong property-structure relationship exists for CNTY arrays and fibers, the mechanical properties of CNTYs reported in the literature present a wide range. For example, Jayasinghe et al. [13] reported an elastic modulus between 1.6 GPa and 6.5 GPa and tensile strength around 168–278 MPa, which agrees with the results obtained herein. In other reports, the engineering elastic modulus of CNTYs has been reported in the range of 6.5–357 GPa, and the tensile strength is within 0.36–1.91 [7,14–16,58,59]. Regarding the textile approach, values around 0.62–0.95 N/tex for the specific strength (tenacity) and 37.4–397 N/tex for the specific modulus have been found reported for other twisted CNTYs [50,59]. From the material viewpoint, the variability stems from the different synthesis methods, lengths of the CNT arrays, and properties of the constituent CNTs, such as inner and outer diameters and number of walls [12]. Structural parameters at the microscale such as porosity and twist angle, as well as test strain rate and gage length are also factors contributing to the strong structure-property relationships of CNTYs. Another source of variability, even within the same yarn, is the selection of the CNTY diameter used for the calculation of the engineering properties. For example, in our case, for $L_g = 25$ mm the elastic modulus yields 1.02 GPa if the lower bound of the diameter distribution of Fig. 3(*b*) is used (32 μm); however, if the upper bound is used instead (56 μm), the elastic modulus yields 3.14 GPa. This corresponds to an uncertainty of ~55%, and ~37% with respect to the elastic modulus obtained with the mean value of diameter (37.9 μm for batch C, see Sec. S1 available in the Supplemental Materials on the ASME Digital Collection). For the case of the textile approach, accurate determination of the linear density is of paramount importance and that should be conducted using more than one CNTY length, and CNTY lengths that are sufficient to comply with the precision of the instrument used for mass measurement, see Fig. 6.

3.4 Dynamic Mechanical Response. The DMA tensile response of the CNTYs as a function of temperature (T) is shown in Fig. 10(*a*). It is observed that the storage modulus (E') decreases from ~100 GPa (specific storage modulus, $E'/\rho =$ 0.27 N/tex) to ~15 GPa ($E'/\rho = 0.04$ N/tex). The loss modulus (E'') varies between 7 GPa (specific loss modulus, $E''/\rho = 0.02$ N/tex) and 18 GPa ($E''/\rho = 0.05$ N/tex). From −50 °C to ~130 °C,

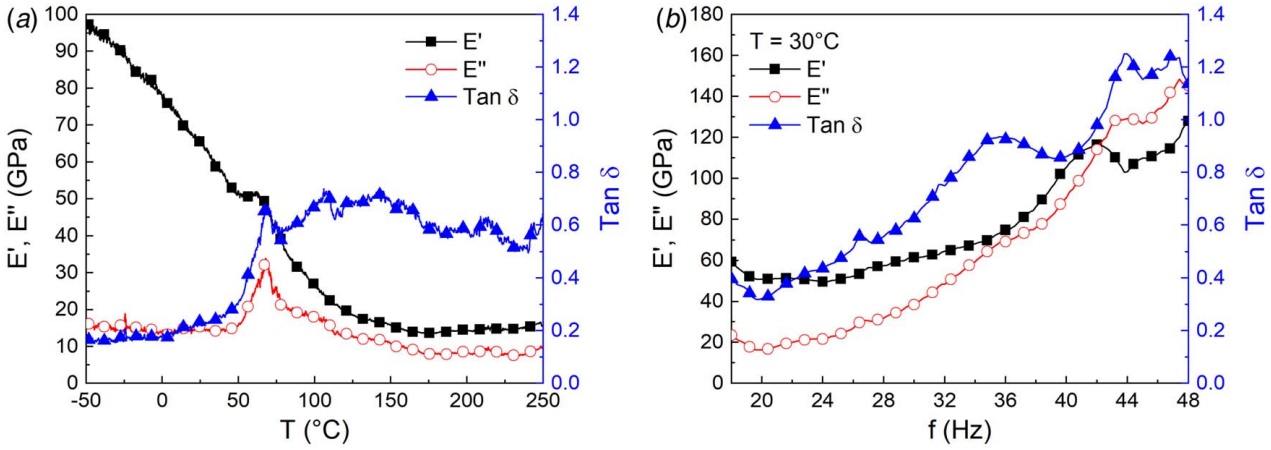

Fig. 10 DMA tensile response of representative CNTYs: (*a*) response as a function of temperature (*T*) and (*b*) response as a function of frequency (*f*)

E' decreases rapidly with increasing temperature. After 130 °C, E' remains almost constant. This quick decrease in E' at low temperatures is different from other materials such as polymers, where E' typically decreases slowly until the glass transition temperature of the polymer [21]. This is because, in the glassy state, polymer segments become more mobile given the softening of the material [60]. In the case of CNT assemblies (CNTYs), the change in E' with temperature is due to restructuring at the CNT and CNT bundle levels [20,21,26]. For the same range of temperatures, the loss modulus (E'') remains nearly constant, which yields a damping ratio ($\text{Tan}(\delta) = E''/E' = (E''/\rho)/(E'/\rho)$) that increases steadily from ~0.2 to ~0.6 up to 60 °C, and then oscillates around ~0.6 for higher temperatures. Notice that 30 DMA tests were conducted in our whole test plan (selected results are shown) and the results showed some degree of specimen-to-specimen scattering, see Fig. S4 available in the Supplemental Materials on the ASME Digital Collection. The variability observed in the dynamic mechanical response is associated with the non-homogeneous fiber architecture, due to the current state of the art of synthesis methods. CNTYs consist of thousands of CNT bundles that are not equally packed, not perfectly uniform, and may comprise several types of CNTs (SWCNTs, DWCNTs, MWCNTs).

It is well known that the damping ratio of traditional materials such as polymers and metals is temperature-dependent due to phase changes (e.g., glass or melt transitions). However, the damping ratio of CNT assemblies, such as CNTYs, depends chiefly on structural changes of its hierarchical structure [21,26]. According to the TGA in Fig. 8, the onset of CNT thermal degradation occurs at around 550 °C, so the sharp changes in E' below 130 °C cannot be explained by material property degradation. Instead, alignment and rearranging of the bundles and fibrils comprising the yarn, sliding, and slippage between bundles/fibrils (stick-slip motions), and zipping/unzipping at CNT connections have been recognized as mechanisms affecting the dynamic mechanical response of CNT assemblies [20,21].

In order to further support this point, additional in situ Raman spectroscopy measurements were conducted while applying tensile strain to the CNTY, using the test rig shown in Sec. S2 available in the Supplemental Materials on the ASME Digital Collection. A 5 μm-long Raman line scan was performed along the axial direction of a CNTY during tensile straining. The CNTY was strained up to 0.83% strain (250 μm) in steps of 50 μm (corresponding to 0.16% strain), and the Raman line scan was performed right after each loading step. Further details can be found in Sec. S2 available in the Supplemental Materials on the ASME Digital Collection. The argument under these dedicated experiments is that the C–C bond stretching of the CNTs that make up the CNTYs should cause a shift in the position of the D or G Raman bands, as has been previously observed for other fibers [61,62]. Our benchmarking tests conducted on Aramid (Twaron) fibers using the same rig and identical methodology yielded conspicuous shifting of the band at ~1610 cm^{-1} with strain, even at small strains. The strain sensitivity of the band at ~1610 cm^{-1} measured for the Twaron fiber was −2.79 cm^{-1}/%, which is in agreement with what has been reported in the literature [61,62]. This indicates a high degree of bond stretching in the molecular structure of the Twaron fiber. On the other hand, for the case of the CNTY investigated herein, the experiments summarized in Sec. S2 available in the Supplemental Materials on the ASME Digital Collection indicate negligible shifting of the Raman bands for strains up to ~0.83%. This experiment confirms that the C–C bond stretching upon axially loading the CNTY to small strains is inexistent or very small. Thus, tensile loading of the CNTY should be governed by the structural mechanisms discussed above (sliding and slippage between CNTs and CNT bundles). This is because less energy is required to break the van der Waals and other secondary bonds and disentangle the yarn bundles than to break the C-C bonds of the CNTs.

All these mechanisms are expected to be affected by temperature. TGA also shows that, if the yarn is not preheated, certain byproducts suffer thermal degradation below 130 °C. Therefore, the thermal transformation of such byproducts may be further affecting the structural changes expected at the bundle level and changing the porosity of the yarn. This phenomenon may facilitate CNT bundles relaxation through sliding [26]. As a result, CNT bundles (and CNTs) begin to orient parallel to the loading direction (the twist angle decreases), decreasing the contacts between CNT bundles and, therefore, the inter-bundle friction. This causes E' to decrease since the load transfer between two adjacent bundles is affected by the number of contacts between them [58]. On the other hand, E'' remains almost constant or with a slightly increasing trend, until a temperature of ~65 °C is reached. This is explained by attachment-detachment of the CNTY bundles originated by the increase and decrease of contact points, until a relatively stable value is reached. Once this critical temperature is reached ($T > 65$ °C in this case), the bundles reach the maximum level of relaxation, so E'' levels off. It may also be possible that some large hydrocarbon chains reside on the surface of the CNTs grown by chemical vapor deposition, and they start to flow around this temperature.

The DMA tensile response of the CNTYs as a function of frequency (f) for $T = 30$ °C is shown in Fig. 10(*b*). Frequency responses for different temperatures are shown in Fig. S5 available in the Supplemental Materials on the ASME Digital Collection. Results indicate a shift of E' towards lower values and of E'' towards higher values as the temperature increases, consistent with the results of Fig. 10(*a*). A frequency-independent response of the yarn with only random oscillations was observed for frequencies smaller than 18 Hz (results not shown). After 18 Hz, both E' and E'' increase with increased frequency, indicating a

frequency-stiffening behavior. The results indicate that energy dissipation mechanisms become more prominent as f increases. E'' has a higher rate of increase (up to ~700% at 48 Hz) than E' (up to ~250% at 48 Hz), which results in the increase of Tan(δ) with increased f. Tan(δ) goes from ~0.40 at 18 Hz to 1.20 at 48 Hz. This is a very high damping ratio, indicating that the CNTY is an outstanding energy dissipation material. Materials with high energy dissipation capabilities have been reported with damping ratios of 0.42 at 200 Hz for CNT arrays [20], ~0.10 at 50 Hz for ethylene glycol-densified CNT fibers [26], and ~0.09 at 10 Hz for nylon yarns [26]. As proved by the in situ Raman spectroscopy reported in Sec. S2 available in the Supplemental Materials on the ASME Digital Collection, the energy dissipation mechanisms are governed by structural (rather than material) mechanisms. During tensile loading/unloading cycles, the CNTs within the bundles are reversibly attached and detached through zipping/unzipping mechanisms [21,63,64]. This mechanism is one of the causes of energy dissipation since the process of unzipping between CNTs and their bundles/fibrils consume energy to overcome the van der Waals forces [63,64], while the zipping process does not require energy consumption [63]. Another mechanism that likely contributes to dissipate energy in the CNTY is the detaching/attaching process [26,64]. Unlike the zipping/unzipping mechanism, the detaching/attaching mechanism irreversibly changes the CNT network morphology during each loading/unloading cycle. The inter-bundle friction plays a very important role in the energy dissipation mechanisms. As contact between the CNT bundles (see AFM in Fig. 4) increases (e.g., by increasing the twist angle or decreasing the porosity), sliding dissipation increases [21,26]. This mechanism is also strain rate-dependent [14]. For low strain rates (i.e., low frequency), the CNT bundles have enough time to align longitudinally and relax [14]. As the frequency increases, the CNTs and CNT bundles relaxation through sliding turns into a slow process compared with the loading rate, and therefore, the strain re-distribution becomes more difficult [14].

4 Conclusions

Carbon nanotube yarns are hierarchical materials with extraordinary specific mechanical properties and very high energy dissipation capabilities. However, the state of the art of their current synthesis methods yields CNTYs with considerable variations in diameter and structural properties, which makes their characterization challenging. The dynamic mechanical analysis (DMA) of the CNTYs tested here showed that CNTYs have extraordinary energy dissipation capabilities, with damping ratios that increase with temperature and reach ~0.6 at 60 °C. The CNTYs presented a frequency-stiffening behavior in the 18–48 Hz range, where the storage modulus and loss modulus increased ~2.5 and ~7 times, respectively. The results suggest that energy dissipation mechanisms are majorly structural (rather than material), including sliding and slippage between CNTs and CNT bundles, inter-bundle friction, zipping/unzipping, and detaching/attaching.

The variability in the structural constitution of the CNTY at the nano-, micro-, and meso-scale levels affects the variability of the effective CNTY properties measured. Raman mapping arises as an ideal and practical tool to assess such structural variability. In our case, line mapping of a 100 μm long section of the fiber, including 101 scans, showed a coefficient of variation in the I_D/I_G ratio of ~5%. The tensile properties of CNTYs depend on the gage length and are affected by the machine compliance. The strength is weakly sensitive to the gage length of the CNTY, while the elastic modulus and ultimate strain depend on the gage length. Accurate determination of the CNTY diameter is crucial for accurate determination of the mechanical and dynamic mechanical properties of the CNTY. Since variations in the CNTY diameter (even within the same batch) could be significant, statistical analysis of the diameter distribution is recommended. In this case, dry-spun CNTYs with mean diameter of 37.9 μm (expected value obtained from a three-parameter Weibull distribution) yielded a specific strength of 0.21–0.34 N/tex, and a specific elastic modulus of 3.59–8.06 N/tex. The strong property-structure relationship evidenced by CNTYs demands that characterizations of this type of CNT arrays are conducted in various zones and with sufficient statistical significance, in order to advance towards standardization of material properties.

Acknowledgment

This material is based upon research supported by the Office of Naval Research Global (ONRG) under Award number N62909-19-1-2119, granted to Dr. FA. Raman spectroscopy and AFM conducted by Dr. Alejandro May-Pat is strongly appreciated, as well as SEM conducted by Santiago Duarte-Aranda. Technical support of Miguel Rivero-Ayala and Javier Cauich-Cupul with mechanical testing is appreciated. Authors greatly appreciate technical comments of Dr. Iván González, Dr. Jandro Abot (The Catholic University of America), and Dr. Shanov Vesselin (University of Cincinnati).

Conflict of Interest

There are no conflicts of interest.

Data Availability Statement

The datasets generated and supporting the findings of this article are obtainable from the corresponding author upon reasonable request.

References

[1] Jiang, K., Li, Q., and Fan, S., 2002, "Spinning Continuous Carbon Nanotube Yarns," Nature, **419**(24), pp. 801–801.
[2] Zhang, M., Atkinson, K. R., and Baughman, R. H., 2004, "Multifunctional Carbon Nanotube Yarns by Downsizing an Ancient Technology," Science, **306**(5700), pp. 1358–1361.
[3] Guo, W., Liu, C., Zhao, F., Sun, X., Yang, Z., Chen, T., Chen, X., Qiu, L., Hu, X., and Peng, H., 2012, "A Novel Electromechanical Actuation Mechanism of a Carbon Nanotube Fiber," Adv. Mater., **24**(39), pp. 5379–5384.
[4] Mikhalchan, A., and Vilatela, J. J., 2019, "A Perspective on High-Performance CNT Fibres for Structural Composites," Carbon, **150**, pp. 191–215.
[5] Sui, X. M., Greenfeld, I., Cohen, H., Zhang, X. H., Li, Q. W., and Wagner, H. D., 2016, "Multilevel Composite Using Carbon Nanotube Fibers (CNTF)," Compos. Sci. Technol., **137**, pp. 35–43.
[6] Miao, M., 2011, "Electrical Conductivity of Pure Carbon Nanotube Yarns," Carbon, **49**(12), pp. 3755–3761.
[7] Anike, J. C., Belay, K., and Abot, J. L., 2019, "Effect of Twist on the Electromechanical Properties of Carbon Nanotube Yarns," Carbon, **142**, pp. 491–503.
[8] Balam, A., Cen-Puc, M., Rodríguez-Uicab, O., Abot, J. L., and Avilés, F., 2020, "Cyclic Thermoresistivity of Freestanding and Polymer Embedded Carbon Nanotube Yarns," Adv. Eng. Mater., **22**(10), p. 2000220.
[9] Zhang, X., Lu, W., Zhou, G., and Li, Q., 2020, "Understanding the Mechanical and Conductive Properties of Carbon Nanotube Fibers for Smart Electronics," Adv. Mater., **32**(5), p. 1902028.
[10] Kim, S., Kim, S., Kim, Y. H., Ku, B. C., and Jeong, Y., 2015, "Enhancement of Electrical Conductivity of Carbon Nanotube Fibers by Copper Sulfide Plating," Fibers Polym., **16**(4), pp. 769–773.
[11] Lee, Y. R., Park, J., Jeong, Y., and Park, J. S., 2018, "Improved Mechanical and Electrical Properties of Carbon Nanotube Yarns by Wet Impregnation and Multi-Ply Twisting," Fibers Polym., **19**(12), pp. 2478–2482.
[12] Jia, J., Zhao, J., Xu, G., Di, J., Yong, Z., Tao, Y., Fang, C., et al., 2011, "A Comparison of the Mechanical Properties of Fibers Spun From Different Carbon Nanotubes," Carbon, **49**(4), pp. 1333–1339.
[13] Jayasinghe, C., Chakrabarti, S., Schulz, M. J., and Shanov, V., 2011, "Spinning Yarn From Long Carbon Nanotube Arrays," J. Mater. Res., **26**(5), pp. 645–651.
[14] Zhang, Y., Zheng, L., Sun, G., Zhan, Z., and Liao, K., 2012, "Failure Mechanisms of Carbon Nanotube Fibers Under Different Strain Rates," Carbon, **50**(8), pp. 2887–2893.
[15] Wu, A. S., Nie, X., Hudspeth, M. C., Chen, W. W., Chou, T. W., Lashmore, D. S., Schauer, M. W., Tolle, E., and Rioux, J., 2012, "Strain Rate-Dependent Tensile Properties and Dynamic Electromechanical Response of Carbon Nanotube Fibers," Carbon, **50**(10), pp. 3876–3881.

[16] Sugano, K., Kurata, M., and Kawada, H., 2014, "Evaluation of Mechanical Properties of Untwisted Carbon Nanotube Yarn for Application to Composite Materials," Carbon, **78**, pp. 356–365.
[17] Wu, A. S., and Chou, T. W., 2012, "Carbon Nanotube Fibers for Advanced Composites," Mater. Today, **15**(7–8), pp. 302–310.
[18] Lu, W., Zu, M., Byun, J. H., Kim, B. S., and Chou, T. W., 2012, "State of the Art of Carbon Nanotube Fibers: Opportunities and Challenges," Adv. Mater., **24**(14), pp. 1805–1833.
[19] Vilatela, J. J., Deng, L., Kinloch, I. A., Young, R. J., and Windle, A. H., 2011, "Structure of and Stress Transfer in Fibres Spun From Carbon Nanotubes Produced by Chemical Vapour Deposition," Carbon, **49**(13), pp. 4149–4158.
[20] Liu, Q., Li, M., Gu, Y., Wang, S., Zhang, Y., Li, Q., Gao, L., and Zhang, Z., 2015, "Interlocked CNT Networks With High Damping and Storage Modulus," Carbon, **86**, pp. 46–53.
[21] Zhao, J., Wang, F., Zhang, X., Liang, L., Yang, X., Li, Q., and Zhang, X., 2018, "Vibration Damping of Carbon Nanotube Assembly Materials," Adv. Eng. Mater., **20**(3), pp. 1–13.
[22] Abot, J. L., Song, Y., Vatsavaya, M. S., Medikonda, S., Kier, Z., Jayasinghe, C., Rooy, N., Shanov, V. N., and Schulz, M. J., 2010, "Delamination Detection With Carbon Nanotube Thread in Self-Sensing Composite Materials," Compos. Sci. Technol., **70**(7), pp. 1113–1119.
[23] Yang, E., Xu, Z., Baniasadi, M., Moreno, S., Yi, H., Di, J., Baughman, R., and Minary-Jolandan, M., 2018, "Tensile Fatigue Behavior of Single Carbon Nanotube Yarns," J. Mater. Sci., **53**(16), pp. 11426–11432.
[24] ASTM International, 1975, *Standard Test Method for Tensile Strength and Young's Modulus for High-Modulus*, ASTM Standard D 3379–75, ASTM International, West Conshohocken.
[25] Carlsson, L. A., Adams, D. F., and Pipes, R. B., 2014, *Experimental Characterization of Advanced Composite Materials*, CRC Press, Boca Raton.
[26] Zhao, J., Zhang, X., Pan, Z., and Li, Q., 2015, "Wide-Range Tunable Dynamic Property of Carbon-Nanotube-Based Fibers," Adv. Mater. Interfaces, **2**(10), p. 1500093.
[27] Min, J., Cai, J. Y., and Wang, L., 2016, "Investigation on Thermal and Cryogenic Behaviour of Carbon Nanotube Spun Yarns Using a Dynamic Mechanical Analyser," J. Mater. Sci., **51**(18), pp. 8434–8441.
[28] D'Agostino, R. B., and Stephens, M. A., 1986, *Goodness-of-Fit Techniques*, Marcel Dekker Inc., Boca Raton.
[29] Miao, M., 2019, *Carbon Nanotube Fiber and Yarns. Production, Properties and Applications in Smart Textiles*, Woodhead Publishing Ltd, Cambridge.
[30] Laurent, C., Flahaut, E., and Peigney, A., 2010, "The Weight and Density of Carbon Nanotubes Versus the Number of Walls and Diameter," Carbon, **48**(10), pp. 2994–2996.
[31] Filleter, T., Bernal, R., Li, S., and Espinosa, H. D., 2011, "Ultrahigh Strength and Stiffness in Cross-Linked Hierarchical Carbon Nanotube Bundles," Adv. Mater., **23**(25), pp. 2855–2860.
[32] Kuznetsov, A. A., Fonseca, A. F., Baughman, R. H., and Zakhidov, A. A., 2011, "Structural Model for Dry-Drawing of Sheets and Yarns From Carbon Nanotube Forests," ACS Nano, **5**(2), pp. 985–993.
[33] Song, W., Gu, A., Liang, G., and Yuan, L., 2011, "Effect of the Surface Roughness on Interfacial Properties of Carbon Fibers Reinforced Epoxy Resin Composites," Appl. Surf. Sci., **257**(9), pp. 4069–4074.
[34] Liu, J., Tian, Y., Chen, Y., and Liang, J., 2010, "Interfacial and Mechanical Properties of Carbon Fibers Modified by Electrochemical Oxidation in (NH4HCO3)/(NH4)2C2O4·H2O Aqueous Compound Solution," Appl. Surf. Sci., **256**(21), pp. 6199–6204.
[35] Antunes, E. F., Lobo, A. O., Corat, E. J., and Trava-Airoldi, V. J., 2007, "Influence of Diameter in the Raman Spectra of Aligned Multi-Walled Carbon Nanotubes," Carbon, **45**(5), pp. 913–921.
[36] Jorio, A., Saito, R., Hafner, J. H., Lieber, C. M., Hunter, M., McClure, T., Dresselhaus, G., and Dresselhaus, M. S., 2001, "Structural (n, m) Determination of Isolated Single-Wall Carbon Nanotubes by Resonant Raman Scattering," Phys. Rev. Lett., **86**(6), pp. 1118–1121.
[37] Cui, S., Kinloch, I. A., Young, R. J., Noé, L., and Monthioux, M., 2009, "The Effect of Stress Transfer Within Double-Walled Carbon Nanotubes Upon Their Ability to Reinforce Composites," Adv. Mater., **21**(35), pp. 3591–3595.
[38] Jorio, A., Pimenta, M. A., Souza Filho, A. G., Saito, R., Dresselhaus, G., and Dresselhaus, M. S., 2003, "Characterizing Carbon Nanotube Samples With Resonance Raman Scattering," New J. Phys., **5**, p. 139.
[39] Lehman, J. H., Terrones, M., Mansfield, E., Hurst, K. E., and Meunier, V., 2011, "Evaluating the Characteristics of Multiwall Carbon Nanotubes," Carbon, **49**(8), pp. 2581–2602.
[40] Dresselhaus, M. S., Dresselhaus, G., Saito, R., and Jorio, A., 2005, "Raman Spectroscopy of Carbon Nanotubes," Phys. Rep., **409**(2), pp. 47–99.
[41] Saito, R., Hofmann, M., Dresselhaus, G., Jorio, A., and Dresselhaus, M. S., 2011, "Raman Spectroscopy of Graphene and Carbon Nanotubes," Adv. Phys., **60**(3), pp. 413–550.
[42] Osswald, S., Havel, M., and Gogotsi, Y., 2007, "Monitoring Oxidation of Multiwalled Carbon Nanotubes by Raman Spectroscopy," J. Raman Spectrosc., **38**(April), pp. 728–736.
[43] Malard, L. M., Pimenta, M. A., Dresselhaus, G., and Dresselhaus, M. S., 2009, "Raman Spectroscopy in Graphene," Phys. Rep., **473**(5–6), pp. 51–87.
[44] Ferrari, A. C., and Basko, D. M., 2013, "Raman Spectroscopy as a Versatile Tool for Studying the Properties of Graphene," Nat. Nanotechnol., **8**(4), pp. 235–246.
[45] Li, Q., Li, Y., Zhang, X., Chikkannanavar, S. B., Zhao, Y., Dangelewicz, A. M., Zheng, L., et al., 2007, "Structure-Dependent Electrical Properties of Carbon Nanotube Fibers," Adv. Mater., **19**(20), pp. 3358–3363.
[46] Pimenta, M. A., Dresselhaus, G., Dresselhaus, M. S., Cançado, L. G., Jorio, A., and Saito, R., 2007, "Studying Disorder in Graphite-Based Systems by Raman Spectroscopy," Phys. Chem. Chem. Phys., **9**(11), pp. 1276–1291.
[47] Kim, K. K., Park, J. S., Kim, S. J., Geng, H. Z., An, K. H., Yang, C. M., Sato, K., Saito, R., and Lee, Y. H., 2007, "Dependence of Raman Spectra G′ Band Intensity on Metallicity of Single-Wall Carbon Nanotubes," Phys. Rev. B, **76**(20), p. 205426.
[48] Villalpando-Paez, F., Son, H., Nezich, D., Hsieh, Y. P., Kong, J., Kim, Y. A., Shimamoto, D., et al., 2008, "Raman Spectroscopy Study of Isolated Double-Walled Carbon Nanotubes With Different Metallic and Semiconducting Configurations," Nano Lett., **8**(11), pp. 3879–3886.
[49] Miao, M., McDonnell, J., Vuckovic, L., and Hawkins, S. C., 2010, "Poisson's Ratio and Porosity of Carbon Nanotube Dry-Spun Yarns," Carbon, **48**(10), pp. 2802–2811.
[50] Vilatela, J. J., and Windle, A. H., 2010, "Yarn-Like Carbon Nanotube Fibers," Adv. Mater., **22**(44), pp. 4959–4963.
[51] Reguero, V., Alemán, B., Mas, B., and Vilatela, J. J., 2014, "Controlling Carbon Nanotube Type in Macroscopic Fibers Synthesized by the Direct Spinning Process," Chem. Mater., **26**(11), pp. 3550–3557.
[52] Shanov, V. N., Gorton, A., Yun, Y. H., and Schulz, M. J., 2008, "Composite Catalyst and Method for Manufacturing Carbon Nanostructured Materials," WO/2008/105936 A2.
[53] Avilés, F., Cauich-Rodríguez, J. V., Moo-Tah, L., May-Pat, A., and Vargas-Coronado, R., 2009, "Evaluation of Mild Acid Oxidation Treatments for MWCNT Functionalization," Carbon, **47**(13), pp. 2970–2975.
[54] Schönfelder, R., Avilés, F., Bachmatiuk, A., Cauich-Rodríguez, J. V., Knupfer, M., Büchner, B., and Rümmeli, M. H., 2012, "On the Merits of Raman Spectroscopy and Thermogravimetric Analysis to Asses Carbon Nanotube Structural Modifications," Appl. Phys. A, **106**(4), pp. 843–852.
[55] Santangelo, S., Lanza, M., and Milone, C., 2013, "Evaluation of the Overall Crystalline Quality of Amorphous Carbon Containing Multiwalled Nanotubes," J. Phys. Chem. C, **117**(9), pp. 4815–4823.
[56] Igbokwe, E. C., Daramola, M. O., and Iyuke, S. E., 2019, "Production of Carbon Nanotube Yarns Via Floating Catalyst Chemical Vapor Deposition: Effect of Synthesis Temperature on Electrical Conductivity," Results Phys., **15**, p. 102705.
[57] Lima, A. M. F., Musumeci, A. W., Liu, H. W., Waclawik, E. R., and Silva, G. G., 2009, "Purity Evaluation and Influence of Carbon Nanotube on Carbon Nanotube/Graphite Thermal Stability," J. Therm. Anal. Calorim., **97**(1), pp. 257–263.
[58] Beese, A. M., Wei, X., Sarkar, S., Ramachandramoorthy, R., Roenbeck, M. R., Moravsky, A., Ford, M., et al., 2014, "Key Factors Limiting Carbon Nanotube Yarn Strength: Exploring Processing-Structure-Property Relationships," ACS Nano, **8**(11), pp. 11454–11466.
[59] Jung, Y., Cho, Y. S., Lee, J. W., Oh, J. Y., and Park, C. R., 2018, "How Can We Make Carbon Nanotube Yarn Stronger?," Compos. Sci. Technol., **166**, pp. 95–108.
[60] Gnanou, Y., and Fontanille, M., 2008, *Organic and Physical Chemistry of Polymers*, John Wiley & Sons, Hoboken, NJ.
[61] Day, R. J., and Cauich Rodrigez, J. V., 1998, "Investigation of the Micromechanics of the Microbond Test," Compos. Sci. Technol., **58**(6), pp. 907–914.
[62] Young, R. J., Lu, D., Day, R. J., Knoff, W. F., and Davis, H. A., 1992, "Relationship Between Structure and Mechanical Properties for Aramid Fibres," J. Mater. Sci., **27**(20), pp. 5431–5440.
[63] Xu, M., Futaba, D. N., Yamada, T., Yumura, M., and Hata, K., 2010, "Carbon Nanotubes With Temperature-Invariant Viscoelasticity From −196° to 1000 ° C," Science, **330**(6009), pp. 1364–1368.
[64] Li, Y., and Kröger, M., 2012, "Viscoelasticity of Carbon Nanotube Buckypaper: Zipping-Unzipping Mechanism and Entanglement Effects," Soft Matter, **8**(30), pp. 7822–7830.